On compensator design for photon beam intensity-modulated conformal therapy

Steve B. Jiang[a] and Komanduri M. Ayyangar
Department of Radiation Therapy, Medical College of Ohio, 3000 Arlington Avenue, Toledo, Ohio 43614-2598

(Received 30 September 1997; accepted for publication 19 February 1998)

Recently the compensator has been shown to be an inexpensive and reliable dose delivery device for photon beam intensity-modulated radiation therapy (IMRT). The goal of IMRT compensator design is to produce an optimized primary fluence profile at the patient's surface obtained from the optimization procedure. In this paper some of the problems associated with IMRT compensator design, specifically the beam perturbations caused by the compensator, are discussed. A simple formula is derived to calculate the optimal compensator thickness profile from an optimized primary fluence profile. The change of characteristics of a 6 MV beam caused by the introduction of cerrobend compensators in the beam is investigated using OMEGA Monte Carlo codes. It is found that the compensator significantly changes the energy spectrum and the mean energy of the primary photons at the patient's surface. However, beam hardening does not have as significant an effect on the percent depth dose as it does on the energy spectrum. We conclude that in most situations the beam hardening effect can be ignored during compensator design and dose calculation. The influence of the compensator on the contaminant electron buildup dose is found to be small and independent of the compensator thickness of interest. Therefore, it can be ignored in the compensator design and included as a correction into the final dose distribution. The scattered photons from the compensator are found to have no effect on the surface dose. These photons produce a uniform low fluence distribution at the patient's surface, which is independent of compensator shape. This is also true for very large fields and extremely asymmetric and nonuniform compensator thickness profiles. Compared to the primary photons, the scattered photons have much larger angular spread and similar energy spectrum at the patient's surface. These characteristics allow the compensator thickness profile and the dose distribution to be calculated from the optimized fluence profile of primary photons, without considering the scattered photons. [S0094-2405(98)01105-5]

Key words: compensator, conformal therapy, Monte Carlo, intensity modulation

I. INTRODUCTION

Historically, the compensator has been used to generate a uniform dose distribution on a specified plane through the middle of the tumor by compensating for the effects of nonflat patient contour, internal tissue heterogeneities, and sometimes beam obliquity. The idea behind the conventional missing tissue or dose compensator design is to produce a dose distribution similar to that obtained from a beam incident perpendicularly onto a flat homogeneous phantom. Recently, the compensator has also been used as one of the delivery devices in photon beam intensity-modulated radiation therapy (IMRT).[1–10] In IMRT, the compensator is used not in the sense of compensating for missing tissue or tissue heterogeneity but as a beam intensity modifier like dynamic jaws or multileaf collimators (MLC). The goal is to achieve dose uniformity throughout the whole target volume and, more importantly, to spare the critical structures according to the dose and dose-volume constraints prescribed by the clinician for a specific patient. It has been shown that the compensator is an inexpensive and feasible way to deliver IMRT dose distributions when using a few (3–5) fixed portals.[5,9,10]

Design of IMRT compensators differs from that of conventional missing tissue or dose compensators in the sense that there is a different goal to achieve. For conventional compensator design, the goal is to achieve a uniform dose on a specified plane within the patient, while for IMRT the compensator design is to produce an optimized primary fluence profile at the patient's surface. The problems associated with IMRT compensator design have not been thoroughly addressed in previous published works.

A major difference between MLC or scanning pattern based IMRT and compensator based IMRT is that the introduction of the compensator inside a radiation field causes some changes in beam characteristics other than intensity (they are referred to as *beam perturbations* in this paper). Basically, the compensator induced beam perturbations include the hardening of the primary photon spectrum, beam contamination from the compensator scattered photons, and the influence of the compensator on contaminant electron dose. Throughout this paper, the terms *primary* and *scattered* photons are defined with respect to the compensator, i.e., the primary photons are those transmitted through the compensator without any interactions and the scattered photons are those that have interacted with, or were generated by, the

compensator. According to these definitions, an open field contains only primary photons and no scattered photons.

The calculation of the compensator thickness profile from an optimized primary fluence profile is straightforward, typically using the exponential attenuation model.[3] However, if the compensator induced beam perturbations are significant, the dose distribution delivered using the calculated compensator may differ significantly from the intended dose distribution. If that is the case, we have to consider the beam perturbations in the compensator design process. This may dramatically complicate the problem. An iterative procedure has to be used to adjust the calculated compensator thickness profile to produce the intended dose distribution. Also the optimization and dose calculation procedures will become much more complex. For example, if the beam hardening has an important effect on the depth dose distribution, and if we use a superposition/convolution type of algorithm for dose calculation, we have to use different dose kernels at different positions in the field. Hence, it is important to investigate the beam perturbations caused by the compensator, not only for the compensator design, but also for developing a proper optimization procedure and dose calculation algorithm.

In the second section of this paper, we discuss a method to calculate the optimal compensator thickness profile from the optimized primary fluence profile while ignoring the beam perturbations. In the third section, the perturbations of a 6 MV photon beam caused by Lipowitz metal (cerrobend) compensators are investigated using the OMEGA Monte Carlo codes.[11] Lipowitz metal is chosen due to its relative high density and large atomic number as compared to other commonly used compensator materials. We expect larger beam perturbations when this material is used for compensator. Some discussion and conclusions are given in the final section.

II. CALCULATION OF THE OPTIMAL COMPENSATOR THICKNESS PROFILE

Usually the optimization process is separated from, and performed before, design of the dose delivery process.[3,9] After the optimization process, we obtain an optimized fluence profile which could produce the intended dose distribution in the patient's body while satisfying the dose-volume constraints. In the optimization procedure a beam is usually divided into many rays, which are actually pencil beams. The pencil beams are well-defined in the sense that all photons within a ray are assumed to (1) move in the same direction along the ray from a point source and (2) have the open field energy spectrum. Therefore, the optimized fluence profile achieved by such an optimization procedure consists of only *primary* photons from an open field. The compensator thickness profile could be derived from this optimized primary fluence profile by simply using the linear attenuation coefficient.[3] However, due to the beam perturbations caused by the compensator, the delivered dose distribution in the patient's body is different from the intended dose distribution. If the difference is significant, an iterative procedure may be needed to tune the calculated compensator thickness profile to finally produce the intended dose distribution. The significance of beam perturbations, and then the necessity of utilizing such an iterative procedure, will be evaluated in the next section. In the present section we discuss a method to calculate the optimal compensator thickness profile from an optimized primary fluence profile while ignoring the beam perturbations.

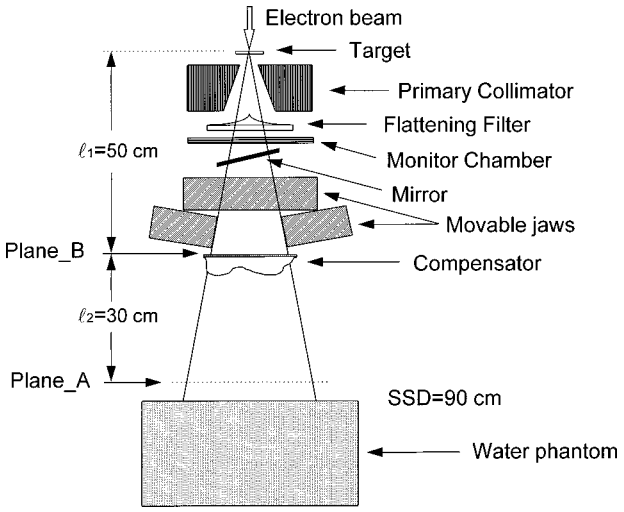

FIG. 1. A schematic illustration of the accelerator treatment head, compensator and water phantom used for Monte Carlo simulation and compensator design.

The exponential model is usually used for compensator attenuation calculation.[3] However, this model introduces unnecessary errors for polyenergetic beams. Actually, the calculation of the transmission data for polyenergetic beams is straightforward, either using analytical methods or Monte Carlo simulation. In the present paper, a primary transmission function $\eta_p(t)$ for a parallel photon beam is precalculated for various thickness of compensator material for a given energy spectrum. (If the off axis softening effect of the beam is considered, η_p should also be a function of the distance from the central axis.) The data are stored in a look-up table and available for interpolation.

During the optimization process the beam is divided into n rays. Initially each ray is assigned a unit fluence $I_0^{(A)}$, then at the end of the process we obtain a weight (or relative fluence), $f_i^{(A)}$, for the ith ray and hence a (relative) primary fluence profile on plane_A (see Fig. 1), $\mathbf{f}^{(\mathbf{A})}$. From this primary fluence profile we can easily calculate the compensator thickness profile if we do not consider the beam perturbations. However, there are an infinite number of thickness profiles corresponding to the same primary fluence profile. So, we have to choose an optimal compensator profile for the given primary fluence profile.

Normally we prefer the thinnest one out of the infinite number of possible compensator profiles, because a thicker compensator introduces larger perturbations to the beam and requires a longer treatment time. Corresponding to the rays, the compensator can be represented with a discretized thickness profile, $\mathbf{t}=[t_i]^T$, $i=1,2,\ldots,n$. Let's assume that the compensator has a minimum feasible thickness t_b (some-

times the compensator has to have a base for mounting purpose) and define the primary transmission ratio for the ith ray as

$$\eta_i = I_0^{(A)} f_i^{(A)} / (I_c^{(B)} f_i^{(B)}), \tag{1}$$

where $I_c^{(B)}$ is the fluence at the central axis on plane_B, and $\mathbf{f^{(B)}} = [f_i^{(B)}]^T$, $i = 1,2,\ldots,n$, is the relative fluence profile on plane_B normalized to $I_c^{(B)}$. Here $\mathbf{f^{(B)}}$ can be calculated with the Monte Carlo method by simulating the treatment head. Notice that η_i is a monotonically decreasing function of the compensator thickness t_i. Assume that the minimum feasible thickness t_b corresponds to a primary transmission ratio η_b for a parallel beam, which gives the maximum possible primary transmission ratio for a divergent beam

$$\eta_i \leqslant \eta_b f_{isl}, \quad i = 1,2,\ldots,n, \tag{2}$$

where $f_{isl} = l_1^2/(l_1+l_2)^2$ is used to take into account beam divergence. Then we have

$$I_c^{(B)} f_i^{(B)} = I_0^{(A)} f_i^{(A)} / \eta_i \geqslant I_0^{(A)} f_i^{(A)} / (\eta_b f_{isl}), \quad i = 1,2,\ldots,n, \tag{3}$$

hence

$$I_c^{(B)} \geqslant I_0^{(A)} f_i^{(A)} / (\eta_b f_{isl} f_i^{(B)}), \quad i = 1,2,\ldots,n. \tag{4}$$

The above equation indicates that the minimum $I_c^{(B)}$ we could use is

$$I_c^{(B)} = \frac{I_0^{(A)}}{\eta_b f_{isl}} \max\{f_i^{(A)}/f_i^{(B)}\}, \quad i = 1,2,\ldots,n, \tag{5}$$

which corresponds to the thinnest compensator profile with the set of maximum possible primary transmission ratios

$$\eta_i = \frac{I_0^{(A)} f_i^{(A)}}{I_c^{(B)} f_i^{(B)}} = \frac{f_i^{(A)}/f_i^{(B)}}{\max\{f_i^{(A)}/f_i^{(B)}\}} \eta_b f_{isl}, \quad i = 1,2,\ldots,n. \tag{6}$$

From the precalculated primary transmission function $\eta_p(t)$ it is easy to calculate the primary transmission ratios for given compensator profile $\mathbf{t} = [t_i]^T, i = 1,2,\ldots,n$,

$$\eta_i = \eta_p(t_i/\cos\theta_i) f_{isl}, \quad i = 1,2,\ldots,n, \tag{7}$$

where θ_i is the angle between the ith ray and the central axis. Finally the optimal compensator profile corresponding to the optimized primary fluence profile, $\mathbf{f^{(A)}}$, is given as

$$t_i = \eta_p^{-1}(\eta_i/f_{isl})\cos\theta_i = \eta_p^{-1}\left[\frac{f_i^{(A)}/f_i^{(B)}}{\max\{f_i^{(A)}/f_i^{(B)}\}} \eta_b\right]\cos\theta_i, \quad i = 1,2,\ldots,n, \tag{8}$$

where $\eta_p^{-1}(\eta)$ denotes the inverse function of $\eta_p(t)$.

III. BEAM PERTURBATIONS CAUSED BY THE COMPENSATOR

A. Methods and materials

OMEGA Monte Carlo codes (BEAM and DOSXYZ) are used to investigate the beam perturbations caused by the presence of a compensator in the field.[11–13] BEAM is based on the EGS4 Monte Carlo code system and is designed to simulate the complicated geometry of radiation therapy units such as linear accelerators.[11] DOSXYZ can use the phase space information generated with BEAM to calculate the dose distributions in a phantom or patient's body.[12,13] We use the Monte Carlo method to study the compensator induced beam perturbations because these problems are difficult or even impossible to address with traditional experimental approaches. In addition, previous studies have shown that the OMEGA codes are able to accurately model the transport of photons and electrons in the accelerator treatment head and generate accurate dosimetric data in a phantom or patient's body.[11,14–17] In our opinion, Monte Carlo simulation based on well established code systems can be used as a reliable and independent data source.

Figure 1 illustrates the simulation setup in the present study. Compensators with material of cerrobend (Lipowitz metal, composed of 13.3% tin, 50% bismuth, 26.7% lead and 10% cadmium by weight, with density of 9.76 g/cm^3) are used to investigate the perturbations to the 6 MV photon beam from a Varian Clinac 1800 accelerator in our institution. All pertinent parts of the accelerator treatment head are modeled with the BEAM code. These parts include the target, primary collimator, flattening filter, monitor chamber, mirror and movable jaws. The compensator is put in the wedge tray at 50 cm from the target with its flat surface toward the source. Two planes are used to score the phase space information generated with the BEAM code. Plane_B is on the compensator upper surface at 50 cm from the source while plane_A is downstream from the compensator at 80 cm distance from the source. A water phantom is placed at 90 cm SSD because for 100 cm SAD conformal treatments the SSD is generally 85–90 cm. For this reason, it is more meaningful to specify the depth dose characteristics for 85 or 90 cm SSD rather than for 100 cm SSD. Information about the locations, physical dimensions and material compositions of the accelerator parts are provided by the manufacturers. The only unknown parameter in the simulations was the *actual* (rather than *nominal*) energy of the electron pencil beam incident on the target which generates the 6 MV photon beam. This energy is determined for our Clinac 1800 machine by matching the Monte Carlo calculated central axis depth dose distribution to the measured depth dose distribution in water for a 10×10 cm^2 open field at 100 cm SSD.[14–17]

First we simulate the accelerator treatment head to get a phase space file on plane_B. This simulation is independent of the compensator and is performed once for each field size. Another simulation is performed by using the phase space file on plane_B as input and modeling the compensator using the BEAM code. The result is another phase space on plane_A at 80 cm from the source. Information we need, such as the fluence distributions, energy spectra, and angular distributions, are extracted from the obtained phase space files. The dose distribution in phantom is calculated with the DOSXYZ code by using the phase space file on plane_A as input. All the simulations in this study are performed on a SGI Indigo 2 platform. Large numbers of photon histories

are used to keep the statistical uncertainty in the results small, e.g., $\sigma<1\%$.

First, the influence of cerrobend compensators with slab geometry on a 6 MV 10×10 cm^2 field is studied. The cerrobend slab thicknesses used are 0.3, 1.2, and 5.0 cm, which roughly correspond to 20%, 50%, and 90% attenuation of a 6 MV photon beam. Usually, conventional missing tissue or dose compensators with attenuation as much as 90% or even 50% are not used. However, in IMRT, sometimes the optimization process prefers part of beam to be strongly attenuated. For example, Stein *et al.* found that the optimization of beam orientations for prostate treatment suggests one posterior-anterior beam. Then, the part of this beam which passes through the rectum should have low intensity.[18] So, in the present study, it is necessary to investigate compensators with large attenuation.

The energy spectra and mean energies on plane_A for primary photons in the fields with and without cerrobend slabs are calculated by simulating the treatment head and cerrobend slabs with the BEAM code. The percent depth dose (PDD) distributions in the water phantom are calculated with the DOSXYZ code. The simulation voxel dimension is 5 mm in the depth direction. The maximum relative standard deviation associated with the results is 0.7%.

As pointed out by Ling and Biggs,[19] the surface dose is a good indicator of buildup characteristics. To investigate the influence of the hardening effect, contaminant electrons, and scattered photons on the surface dose in the presence of cerrobend slabs, we calculate the dose to a 1 mm water layer under the phantom surface and normalize it to the dose at $d_{\max}$. For each slab compensator field, we calculate the (percent) surface dose for three beams: (1) only primary photons, (2) all the photons (primary + scattered), and (3) all the particles (primary photons + scattered photons + electrons). The difference between the surface dose of all photons and primary photons is the contribution from the compensator scattered photons. The contribution from the contaminant electrons is obtained by subtracting the surface dose of all photons from that of all particles. The relative standard deviations of the calculated surface doses are in the range of 0.4% to 0.6%.

It is known that the compensator scattered photons have low spatial frequency. We assume that the compensator scattered photons form a uniform low fluence background at the patient's surface. To check this assumption we simulate the cerrobend compensators with two geometries in a 10×10 cm^2 field. One is a conical geometry with its base at 50 cm from and towards the source. The height of the conical compensator is 5 cm and the base diameter is also 5 cm which projects a circle of 10 cm diameter at isocenter level. The other is a 5 cm thick half-beam block with it upper surface at plane_B. A half-beam block can be thought of as a compensator with extremely asymmetric and nonuniform thickness profile. Then, it is a very stringent test to our assumption of uniform low scattering background. The relative fluence distributions of primary and scattered photons on plane_A for both geometries are calculated. We also calculate the angular distributions and energy spectra of primary and scattered photons on plane_A for the conical geometry.

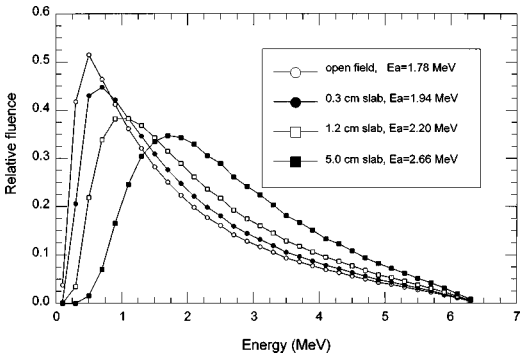

FIG. 2. Energy spectra of primary photons of a 6 MV beam on plane_A for 10×10 cm^2 open and compensated fields. The compensators are cerrobend slabs of thicknesses of 0.3, 1.2, and 5.0 cm. Each energy spectrum is normalized to have a unit area under the curve. E_a represents the mean energy.

It is expected that for very large fields, the uniformity of the scattered photon fluence distribution might be reduced. To test the large field limit of our assumption, we simulate a 35×35 cm^2 field for both conical and half-beam block geometries, even though this large field size is usually not used in conformal therapy. The conical geometry has a 17.5 cm base diameter and a 5 cm height. The half-beam block has the same height. The relative fluence distributions of primary and scattered photons on plane_A are obtained from the corresponding phase space files.

B. Results

The energy spectra and mean energies on plane_A for primary photons after the cerrobend slabs of three different thickness and those in the open field are given in Fig. 2. All the spectra are normalized to have unit areas under the curves. It is found that low energy photons are filtered by the slabs and the energy spectrum hardening is obvious. For the open field, the photon mean energy is 1.78 MeV. For compensated fields the mean energies of the primary photons are 1.94, 2.20, and 2.66 MeV for slab thicknesses of 0.3, 1.2, and 5.0 cm, respectively. Compared to the open field, the mean energy increases by 9%, 24%, and 49% due to the hardening effect of these slabs.

Figure 3 shows the percent depth dose (PDD) distributions in the water phantom for primary photons from the open and slab fields. Due to beam hardening the PDD after $d_{\max}$ is larger for compensated fields than for the open field. After $d_{\max}$ the PDD augmentation caused by beam hardening increases with slab thickness. Also, for the same slab thickness, this augmentation increases with depth. At 10 cm in water, the compensator causes the increases in the primary photon PDDs by approximately 1%, 2%, and 3% for 0.3, 1.2, and 5.0 cm thick slabs, respectively. These increases are much smaller than the increases in beam mean energy on plane_A. It indicates that the PDD curve is not sensitive to the change in the beam energy spectrum at the patient's surface.

Figure 4 shows the calculated surface dose as a function of cerrobend slab thickness for various beam compositions.

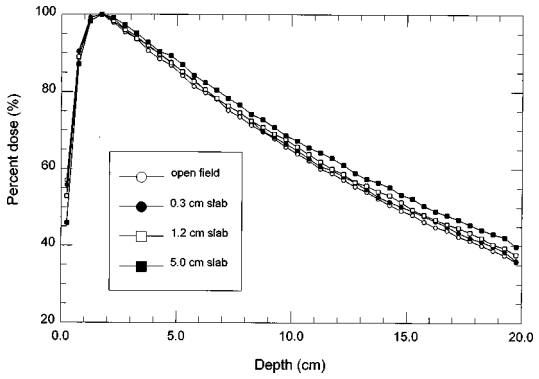

FIG. 3. Percent depth dose distributions of primary photons of a 6 MV beam in water (SSD=90 cm) for 10×10 cm^2 open and compensated fields. The compensators are cerrobend slabs of thicknesses of 0.3, 1.2, and 5.0 cm.

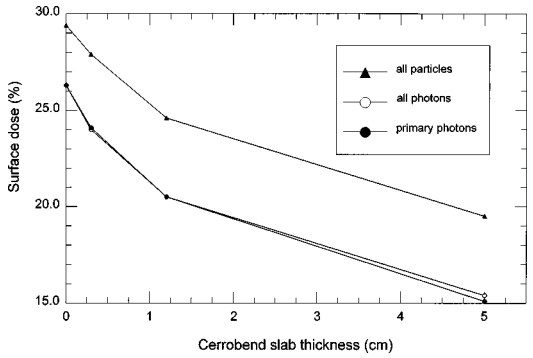

FIG. 4. Surface dose of a 10×10 cm^2 6 MV photon beam in water (SSD=90 cm) as a function of cerrobend slab thickness for various beam compositions.

The surface dose decreases with slab thickness due to the beam hardening effect. The amount of decrease is about 2%, 5%, and 10% for cerrobend slabs with thicknesses of 0.3, 1.2, and 5.0 cm, respectively. This indicates that beam hardening has a larger effect on the surface dose than on the dose at 10 cm depth. The contribution of the compensator scattered photons to the surface dose is negligible. Even for a very large cerrobend slab thickness (5 cm), their contribution to the surface dose is only 0.3%. The contribution of contaminant electrons to the surface dose is about 3% for the open field (slab thickness = 0 cm) and 4% for all the compensated fields. So, the compensator only increases the contaminant electron surface dose by about 1% of the maximum dose. The compensator (or other beam filters) has three major effects on contaminant electrons, which are (1) the absorption of the contaminant electrons generated by the treatment head above the compensator, (2) the generation of new contaminant electrons by the interactions of photons with the compensator, and (3) the self-absorption of the compensator generated electrons. So, the curve of the contaminant electron surface dose versus slab thickness can be divided into three regions. For a very thin compensator slab, with the increase of slab thickness the amount of contaminant electrons decreases, because more treatment head generated electrons are absorbed by a thicker compensator while the compensator does not produce enough new electrons to compensate. With the continuous increase of slab thickness the process of the compensator generating new electrons dominates, so the amount of contaminant electrons begins to increase. When the compensator thickness exceeds a certain value (approximately the electron range in the compensator material), the surface dose of the contaminant electrons does not vary with compensator thickness. This is because the compensator stops all the treatment head electrons while the compensator generation and self-absorption of electrons reach an equilibrium. Figure 4 indicates that the influence of the compensator on the contaminant electron surface dose is small and does not vary with compensator thickness investigated.

The relative fluence distribution of primary and scattered photons at plane_A for a beam opening of 10×10 cm^2 with a conical cerrobend compensator is given in Fig. 5. It is found that the fluence of the compensator scattered photons is low and uniformly distributed over the whole field, even though from the central axis to the beam edge the primary photon fluence varies by a factor of 10. Figure 6 shows the relative fluence distribution of primary and scattered photons at plane_A for a 10×10 cm^2 field and a cerrobend half-beam block. We can see that the fluence distribution of compensator scattered photons is still very uniform. This indicates that even for compensators with extremely asymmetric and nonuniform thickness profiles, our assumption about uniform low scattering background is still correct.

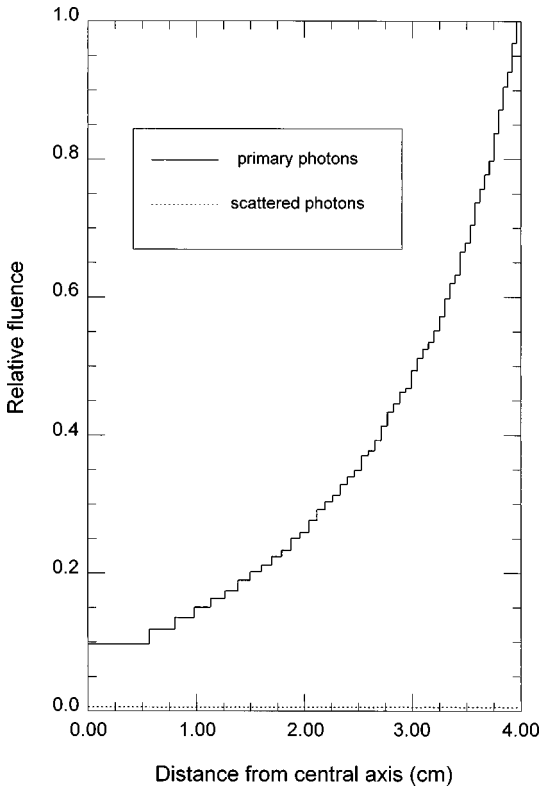

FIG. 5. Relative fluence distribution on plane_A for primary and scattered photons of a 10×10 cm^2 6 MV beam after a cerrobend conical compensator with its base at 50 cm from and towards the source. The height and base diameter of the conical compensator are both 5 cm.

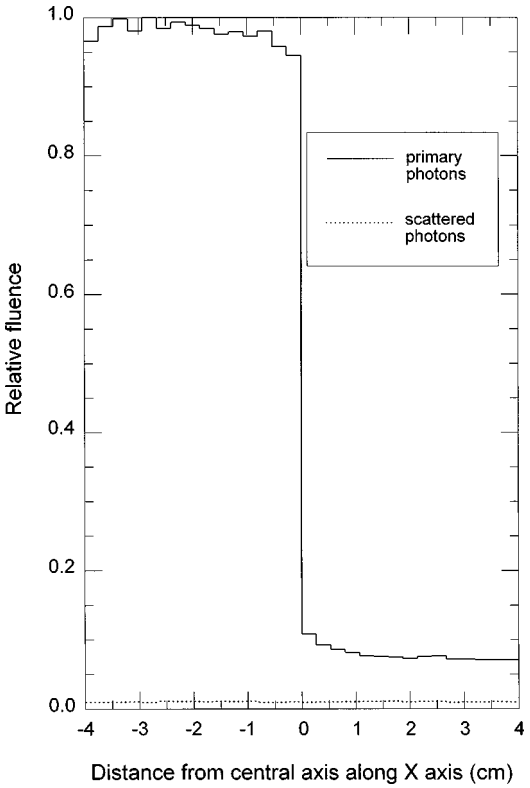

FIG. 6. Relative fluence distribution on plane_A for primary and scattered photons of a 10×10 cm^2 6 MV beam after a cerrobend half-beam block with its upper surface at 50 cm from the source. The thickness of the half-beam block is 5 cm.

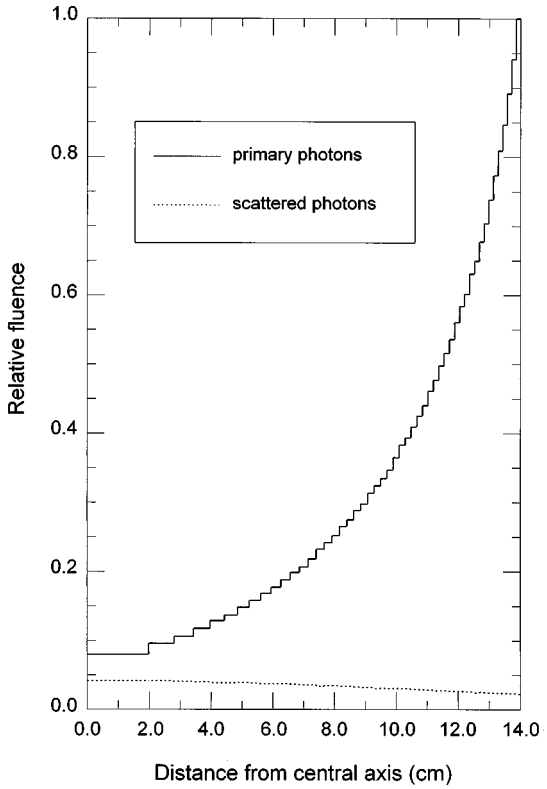

FIG. 7. Relative fluence distribution on plane_A for primary and scattered photons of a 35×35 cm^2 6 MV beam after a cerrobend conical compensator with its base at 50 cm from and towards the source. The height of the conical compensator is 5 cm and the base diameter is 17.5 cm.

Figures 7 and 8 give the relative fluence distributions on plane_A for a 35×35 cm^2 field and for a conical compensator with 17.5 cm base diameter and 5 cm height and a half-beam block of 5 cm thickness, respectively. As we can see, the uniformity of the scattered photon fluence distribution is reduced for this very large field compared to the 10×10 cm^2 field; under the thicker parts of the compensator we get more scattered photons. However, this reduction is not significant. For the conical geometry the relative scattered photon fluence decreases from 4.2% at the central axis to 2.2% at beam edge while the relative primary photon fluence increases from 8% to 100%. For the half-beam block, the ratio of fluence in the open to blocked half of the field is about 20 for primary photons and about 0.4 for scattered photons. So even for very large field sizes there is no strong correlation between the scattered photon fluence distribution and the compensator shape, and our assumption of uniform low scattering fluence background still holds.

Figure 9 shows the angular distributions of primary and scattered photons on plane_A for a conical geometry and a 10×10 cm^2 field. The angle here is defined as the angle between the direction of photon motion and the ray direction from a point source. Both distributions are normalized to their own maximum values. It is interesting to find that the primary photon angular distribution is very narrow. As mentioned earlier, in this work the primary photons are defined with respect to the compensator, so they include the scattered photons from all accelerator components except for the compensator. The very narrow angular distribution of primary photons suggests that (1) the point source model used in the optimization and compensator design procedures is a good approximation as long as the dose points at the beam edge do not play an important role in these procedures and (2) the photons scattered from other accelerator components such as movable jaws do not have an appreciable effect on the primary photon angular distribution within a compensator field. On the other hand, we find that the photons scattered from the compensator have a very broad angular spread, up to 9° relative to the ray direction. This broad angular distribution of the scattered photons at least partly explains the observed uniform spatial distribution of the scattered photon fluence. The energy spectra of primary and scattered photons are given in Fig. 10. Both spectra are normalized to have unit areas under the curves. It is found that the scattered photon energy spectrum is not much different from that of primary photons except that some photons with energies about 4–6 MeV are scattered to about 1–2 MeV by the compensator.

IV. DISCUSSION AND CONCLUSIONS

Problems associated with the calculation of the optimal (thinnest) compensator thickness profile from an optimized primary fluence profile have been discussed. Various factors such as the open beam intensity nonuniformity and compensator minimum thickness have been considered. A simple formula has been derived based on a precalculated primary transmission function. However, as the introduction of a

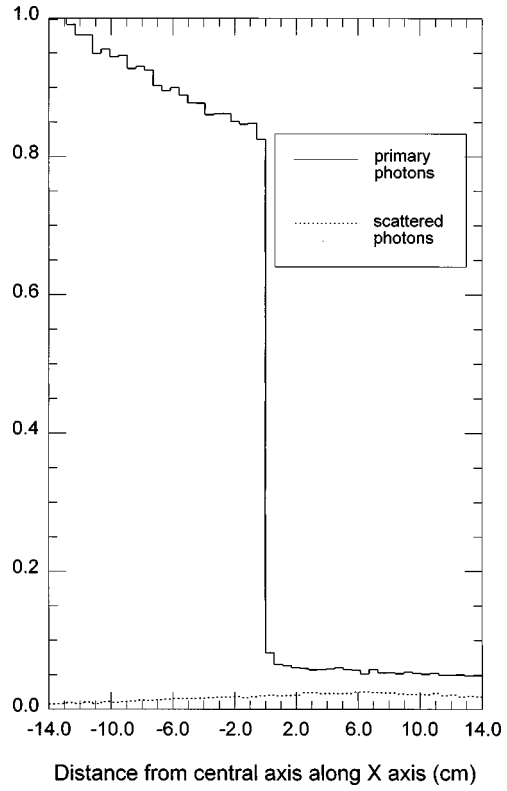

FIG. 8. Relative fluence distribution on plane_A for primary and scattered photons of a 35×35 cm^2 6 MV beam after a cerrobend half-beam block with its upper surface at 50 cm from the source. The thickness of the half-beam block is 5 cm.

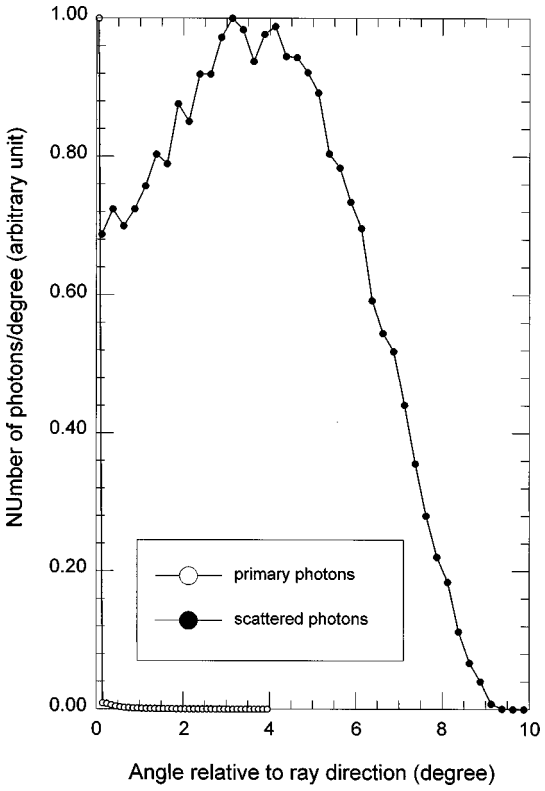

FIG. 9. Angular distributions on plane_A for primary and scattered photons of a 10×10 cm^2 6 MV beam after a cerrobend conical compensator with its base at 50 cm from and towards the source. The height and base diameter of the conical compensator are both 5 cm. The angle is defined as the angle between the direction of photon motion and the ray direction from a point source. Both distributions are normalized to their own maximum values.

compensator into the field alters the beam characteristics in addition to the intensity, the dose distribution delivered by the calculated compensator differs from the intended dose distribution. Hence, the significance of the beam perturbations caused by the compensator has also been investigated using the OMEGA Monte Carlo code system for a 6 MV beam and cerrobend compensators.

It is found that the presence of the compensator hardens the energy spectrum and increases the mean energy of primary photons at the patient's surface significantly. A 5.0 cm cerrobend slab increases the beam mean energy by almost 50%. The beam hardening effect of the compensator also increases the percent depth dose (PDD) after $d_{\max}$ and decreases the surface dose in the patient's body. However, as PDD is not very sensitive to the change of beam energy spectrum, the change in PDD caused by beam hardening is not as significant as that of beam mean energy. For a 6 MV 10×10 cm^2 beam with cerrobend slabs of 0.3, 1.2, and 5.0 cm thick, the decrease of surface dose is about 2%, 5%, and 10% of the maximum dose, and the increase of PDD at 10 cm is about 1%, 2%, and 3% of the maximum dose. Assuming that compensators with large attenuation are not commonly used, in most situations it might be acceptable to design a compensator and calculate the dose distribution without taking into account the beam hardening effect. For example, assuming that the majority of a compensator has attenuation of less than 50% and the tumor is located about 10 cm below the skin, the dose distribution calculated using the optimized primary fluence profile with the open field energy spectrum will have errors less than 2% inside the tumor and 5% near patient's skin. Another fact is that the larger error produced by the thicker part of the compensator will be diluted in the final dose distribution because the corresponding beam rays have lower intensity and multiple fields are used in IMRT. On the other hand, a compensator

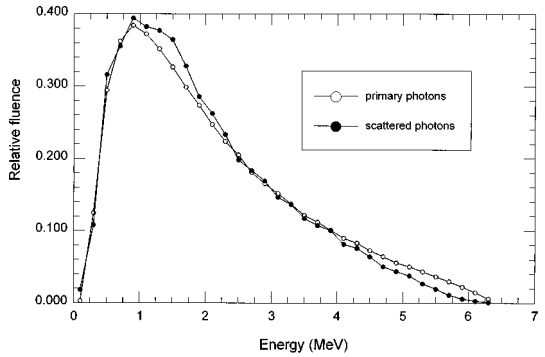

FIG. 10. Energy spectra on plane_A for primary and scattered photons of a 10×10 cm^2 6 MV beam after a cerrobend conical compensator with its base at 50 cm from and towards the source. The height and base diameter of the conical compensator are both 5 cm. Each energy spectrum is normalized to have a unit area under the curve.

with too large a thickness variation may be forbidden in the fabricating procedure. Therefore, it might be a good idea to add a constraint in the optimization algorithm to make sure that the resulted fluence profile does not vary too much across the field.

The surface dose due to the contaminant electrons is about 3% for the open field and 4% for all the investigated fields with cerrobend slabs. The compensator does not significantly distort the dose component of the contaminant electrons. The small change of electron dose due to the compensator is almost independent of compensator thickness. Hence, this effect can be ignored in compensator design and included in the final dose calculation as a correction.

The scattered photons from the compensator have no effect on the surface dose. They produce a uniform low fluence distribution at the patient's surface, which is almost independent of the compensator shape even for very large fields and extremely asymmetric and nonuniform compensator thickness profiles. The scattered photons also have a large angular spread and similar energy spectrum at the patient's surface compared to primary photons. The above characteristics of scattered photons at the patient's surface suggest a uniform low scattering dose background in the patient's body and negligible distortion of the relative dose distribution inside the field. So, the compensator thickness profile and dose distribution can be calculated from the optimized fluence profile of primary photons without the necessity of considering the scattered photons.

The angular distribution of primary photons (including scatter from the treatment head) at the patient's surface is also investigated for a 6 MV 10×10 cm^2 field with a cerrobend compensator of conical geometry. It is found that almost all the primary photons move along the ray direction, which indicates that the point source model can be used in the process of compensator design.

In summary, it is found that the presence of the cerrobend compensators do not significantly affect the characteristics of a 6 MV beam other than intensity. In other words, the compensator thickness profile can be simply calculated from the optimized primary fluence profile without taking into account the beam perturbations caused by the compensator. The dose distribution delivered by the calculated compensator profile should be close enough to the intended dose distribution.

ACKNOWLEDGMENTS

The authors are grateful to Dr. Francesc Salvat of Universitat de Barcelona, Dr. Lech Papiez of Indiana University and Dr. Chen-Shou Chui of Memorial Sloan-Kettering Cancer Center for helpful discussions. The authors also want to thank Todd Pawlicki and Robert Price for comments on the manuscript.

[a]Electronic mail: sjiang@magnum.mco.edu

[1]F. Brix, R. Christiansen, C. Hancken, and A. Quirin, ''The field integrated dose modification (FIDM): three typical clinical applications of a new irradiation technique,'' Radiother. Oncol. **12**, 199–207 (1988).

[2]W. D. Renner, T. P. O'Connor, and N. M. Bermudez, ''An algorithm for design of beam compensators,'' Int. J. Radiat. Oncol., Biol., Phys. **17**, 227–234 (1989).

[3]A. Djordjevich, D. J. Bonham, and E. M. A. Hussein, ''Optimal design of radiation compensators,'' Med. Phys. **17**, 397–404 (1990).

[4]K. J. Weeks and M. R. Sontag, ''3-D dose volume compensation using nonlinear least squares regression technique,'' Med. Phys. **18**, 474–480 (1991).

[5]S. Sodertrom and A. Brahme, ''Optimization of the dose delivery in a few field techniques using radiobiological objective functions,'' Med. Phys. **20**, 1201–1210 (1993).

[6]T. Cullip, A. Jones, S. X. Chang, and E. Chaney, ''A new approach to achieve treatment volume dose homogeneity using compensators,'' Med. Phys. **21**, 938 (1994).

[7]A. Gustafsson, B. K. Lind, R. Svensson, and A. Brahme, ''Simultaneous optimization of dynamic multileaf collimation and scanning patterns or compensation filters using a generalized pencil beam algorithm,'' Med. Phys. **22**, 1141–1156 (1995).

[8]E. P. Miller, S. X. Chang, J. Rosenman, and T. Cullip, ''Dose gradient optimization via compensator: construction and clinical quality assurance,'' Med. Phys. **23**, 1170 (1996).

[9]J. Stein, K. Hartwig, S. Levegrün, G. Zhang, K. Preiser, B. Rhein, J. Debus, and T. Bortfeld, ''Intensity-modulated treatments: compensators vs. multileaf modulation,'' in *Proceedings of The 12th International Conference on The Use of Computers in Radiation Therapy*, Salt Lake City, UT, 1997, edited by D. D. Leavitt and G. Starkschall (Medical Physics, Madison, WI, 1997), pp. 338–341.

[10]O. C. L. Haas, J. A. Mills, K. J. Burnham, D. E. Bonnett, and A. R. Farajollahi, ''Achieving conformal dose distribution via patient specific compensators,'' in *Proceedings of The 12th International Conference on The Use of Computers in Radiation Therapy*, Salt Lake City, UT, 1997, edited by D. D. Leavitt and G. Starkschall (Medical Physics, Madison, WI, 1997), p. 483.

[11]D. W. O. Rogers, B. A. Faddengon, G. X. Ding, C. M. Ma, J. We, and T. R. Mackie, ''BEAM: A Monte Carlo code to simulate radiotherapy treatment units,'' Med. Phys. **22**, 503–524 (1995).

[12]D. W. O. Rogers and A. F. Bielajew, ''Monte Carlo techniques of electron and photon transport for radiation dosimetry,'' in *The Dosimetry of Ionizing Radiation*, edited by K. R. Case, B. E. Bjarngard, and F. H. Attix (Academic, New York, 1990), Vol. 3, pp. 427–539.

[13]A. F. Bielajew and D. W. O. Rogers, ''A standard timing benchmark for EGS4 Monte Carlo calculations,'' Med. Phys. **19**, 303–304 (1992).

[14]K. M. Ayyangar and S. B. Jiang, ''Calculation of dosimetric data for small field sizes for 6 MV x-rays using BEAM/DOSXYZ Monte Carlo codes,'' Med. Phys. **23**, 1129 (1996).

[15]S. B. Jiang and K. M. Ayyangar, ''Characteristics of radiosurgery beams from a Clinac 1800 accelerator: a Monte Carlo study,'' in *Proceedings of The 12th International Conference on The Use of Computers in Radiation Therapy*, Salt Lake City, UT, 1997, edited by D. D. Leavitt and G. Starkschall (Medical Physics, Madison, WI, 1997), pp. 86–87.

[16]K. M. Ayyangar and S. B. Jiang, ''An investigation on the feasibility of using OMEGA Monte Carlo codes for radiosurgery treatment planning,'' in *Proceedings of The 12th International Conference on The Use of Computers in Radiation Therapy*, Salt Lake City, UT, 1997, edited by D. D. Leavitt and G. Starkschall (Medical Physics, Madison, WI, 1997), pp. 88–89.

[17]S. B. Jiang, S. N. Rustgi, A. K. Rustgi, and K. M. Ayyangar, ''Monte Carlo and experimental study of the perturbation caused by inhomogeneity in radiosurgical fields,'' in *Proceedings of The 12th International Conference on The Use of Computers in Radiation Therapy*, Salt Lake City, UT, 1997, edited by D. D. Leavitt and G. Starkschall (Medical Physics, Madison, WI, 1997), p. 485.

[18]J. Stein, R. Mohan, X. H. Wang, T. Bortfield, Q. Wu, K. Preiser, C. C. Ling, and W. Schlegel, ''Number and orientations of beams in intensity-modulated treatments,'' Med. Phys. **24**, 149–160 (1997).

[19]C. C. Ling and P. J. Biggs, ''Improving the buildup and depth-dose characteristics of high energy photon beams by using electron filters,'' Med. Phys. **6**, 296–301 (1979).